Both daughter cells traffic and exocytose membrane at the cleavage furrow during mammalian cytokinesis

John W. Goss and Derek K. Toomre

Department of Cell Biology, Yale University School of Medicine, New Haven, CT 06510

Membrane trafficking during cytokinesis is not well understood. We used advanced live cell imaging techniques to track exocytosis of single vesicles to determine whether constitutively exocytosed membrane is focally delivered to the cleavage furrow. Ultrasensitive three-dimensional confocal time-lapse imaging of the temperature-sensitive membrane cargo protein vesicular stomatitis virus protein–yellow fluorescent protein revealed that vesicles from both daughter cells traffic out of the Golgi and into the furrow, following curvilinear paths. Immunolocalization and photobleaching experiments indicate that individual vesicles accumulate at the midbody and generate a reserve vesicle pool that is distinct from endosomal and lysosomal compartments. Total internal reflection fluorescence microscopy imaging provided direct evidence that Golgi-derived vesicles from both daughter cells not only traffic to the furrow region but dock and fuse there, supporting a symmetrically polarized exocytic delivery model. In contrast, quantitative analysis of midbody abscission showed inheritance of the midbody remnant by one daughter cell, indicating that cytokinesis is composed of both symmetrical and asymmetrical stages.

Introduction

Cytokinesis is the essential process at the termination of cell division resulting in the formation of two daughter cells (Glotzer, 2005). This complex partitioning process involves >100 cellular proteins associated with the cytoskeleton, membrane traffic, and signaling (Skop et al., 2004, Eggert et al., 2006). In mammalian cells, actin and microtubule cytoskeletons play an essential role in the early stages of cytokinesis through contraction of the actinomyosin ring and furrow stabilization, respectively (Finger and White, 2002; Glotzer, 2005).

Although polarized membrane secretion is well accepted to play a central role in plant cytokinesis (Staehelin and Hepler, 1996; Jurgens, 2005), the role of membrane trafficking during animal cytokinesis, although suspected (Finger and White, 2002), is poorly understood. Recent evidence indicates that membrane organelles and exo-endocytic traffic localize to the cleavage furrow during cytokinesis (Lecuit and Wieschaus, 2000; Skop et al., 2001; Danilchik et al., 2003). Moreover, key exocytic and endocytic membrane trafficking machinery, including exocyst subunits, SNARE proteins, dynamin, and clathrin, localize near the midbody (Low et al., 2003; Gromley et al., 2005; Konopka et al., 2006; Warner et al., 2006).

A functional role for exo-endocytic trafficking in cytokinesis was supported by the observation that disrupting the aforementioned machinery can prevent or delay cytokinesis (Niswonger and O'Halloran, 1997; Low et al., 2003; Gromley et al., 2005; Chen et al., 2006; Konopka et al., 2006). Although these studies implicate membrane trafficking in cytokinesis, indirect secondary effects are a potential concern and it is not clear where, when, and which intracellular membrane compartments are involved, as both recycling endosomes (Schweitzer et al., 2005; Wilson et al., 2005; Chen et al., 2006) and exocytic vesicles (Hill et al., 2000; Gromley et al., 2005) are present in the furrow. A critical timely issue is to determine whether exocytosis of post-Golgi vesicles, which encompasses both vesicle trafficking and fusion, occurs selectively at the furrow.

A recent study used spinning disc confocal microscopy (SDCM) to visualize trafficking of fluorescently labeled secretory vesicles in Hela cells during cytokinesis (Gromley et al., 2005). As fluorescent punctae appeared and disappeared asymmetrically

Correspondence to Derek K. Toomre: derek.toomre@yale.edu

Abbreviations used in this paper: DIC, differential interference contrast; EMMA, exocytic midzone membrane accumulation; GPI, glycosylphosphatidylinositol; ROI, region of interest; SDCM, spinning disc confocal microscopy; TGN, trans-Golgi network; TIRFM, total internal reflection fluorescence microscopy; VSVG, vesicular stomatitis virus glycoprotein.

The online version of this paper contains supplemental material.

J. Cell Biol. Vol. 181 No. 7 1047–1054
www.jcb.org/cgi/doi/10.1083/jcb.200712137

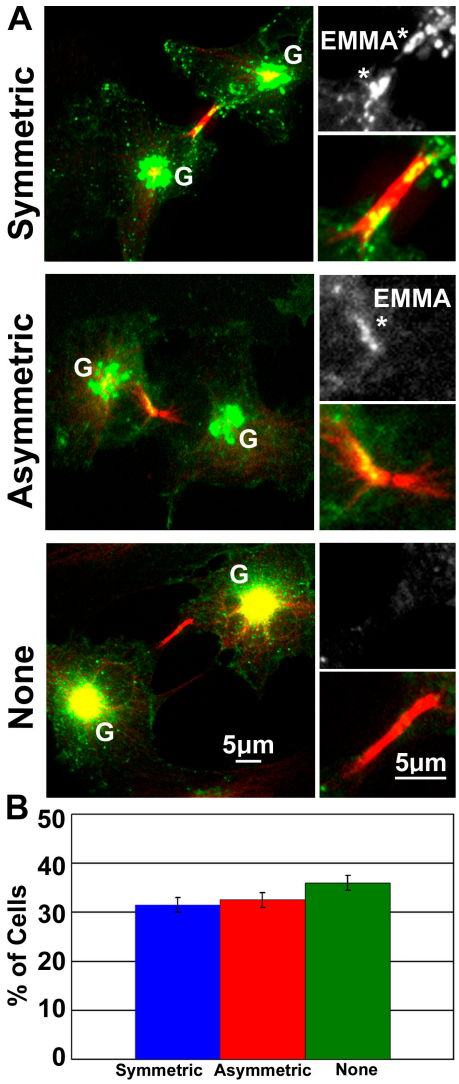

Figure 1. **Post-Golgi membrane accumulates in the cleavage furrow of cells undergoing cytokinesis.** (A) BSC1 cells expressing VSVG-YFP were fixed 60 min after transfer to permissive temperature (32°C) and immunostained with α-tubulin (red). The number of cells with accumulations of VSVG-YFP (green)–labeled post-Golgi membrane in the furrow was evaluated. Boxed regions are enlarged in adjacent panels and show VSVG alone and VSVG/tubulin merge. G, Golgi; asterisks, VSVG EMMAs in the furrow. (B) Manual scoring of symmetric, asymmetrical, and no accumulation of VSVG-labeled membrane in the furrow was quantified in 100 cells. Error bars show SD.

near the furrow over tens of minutes, the authors proposed a model of asymmetrical cell division, whereby one of the two daughter cells selectively traffics vesicles to the cleavage furrow (Gromley et al., 2005). Although intriguing, the relatively low temporal and spatial resolution of prior studies made it impossible to unequivocally trace the complex trafficking itinerary of exocytic vesicles in this process. Moreover, "satellite" Golgi (Gaietta et al., 2006) and recycling endosomes (Schweitzer et al., 2005) were reported to localize near the furrow in some cells, raising the possibility that these and/or other structures may be involved in cytokinesis.

Essential outstanding questions regarding mammalian membrane traffic and cytokinesis include the following: do one or both daughter cells traffic membrane to the furrow? Is the furrow-associated vesicular membrane derived from endosomes, lysosomes, Golgi/trans-Golgi network (TGN), or Golgi-derived vesicles? If the latter, are they clusters of vesicles, as has been previously postulated (Gromley et al., 2005), or does it represent a larger de novo compartment akin to the plant "phragmoplast?" What is the ultimate fate of the abscised midbody, as contradictory evidence suggests that it may be inherited to one daughter cell (Mishima et al., 2002; Gromley et al., 2005) or potentially discarded into the extracellular space (Golsteyn et al., 1994; Hinchcliffe, 2005)?

These questions require high spatial and temporal resolution imaging of individual vesicle trafficking, docking, and fusion during cytokinesis and quantitative analysis of the fate of the midbody. To address the polarization, symmetry, and trafficking of constitutive exocytosis relative to the cleavage furrow, we used temperature-sensitive fluorescent reporters (vesicular stomatitis virus glycoprotein [VSVG]–YFP) and ultrasensitive live cell imaging by SDCM and total internal reflection fluorescence microscopy (TIRFM). Our 3D time-lapse (4D) SDCM and photobleaching experiments showed that both daughter cells traffic vesicles into the furrow where they accumulate and form a reserve membrane pool. Quantification of single exocytic events directly showed polarized fusion in and around the cleavage furrow. Interestingly, differential interference contrast (DIC) microscopy and immunofluorescence analysis support asymmetrical inheritance of the midbody remnant in BSC1 and Hela cells, indicating that cytokinesis is composed of both symmetric and asymmetrical stages.

Results and discussion

Variations in post-Golgi membrane accumulations in the cleavage furrow

To evaluate localization of post-Golgi exocytic cargo during cytokinesis, we used a YFP-tagged temperature-sensitive membrane cargo protein, VSVG-YFP. At 39.5°C, the labeled protein is blocked in the ER and can be released in a synchronous pulse-chase manner at 32°C (Toomre et al., 2000). 1 h after release of VSVG-YFP to the permissive temperature in BSC1 cells, fluorescent labeling is seen in several regions: the Golgi (Fig. 1, G), cell surface (verified by anti-VSVG immunostaining; not depicted), intracellular vesicles, and bright punctae in the cleavage furrow region (Fig. 1, asterisks). The latter fluorescently labeled exocytic midzone membrane accumulations (EMMAs) were present in the cleavage furrow of 63% of cells undergoing cytokinesis (Fig. 1).

To determine whether these accumulations are akin to satellite Golgi twins, which are observed to be proximal to the furrow in Hela and CHO cells (Shima et al., 1998; Skop et al., 2004; Gaietta et al., 2006), or a post-Golgi compartment, we examined colocalization of VSVG-YFP with Golgi (GM130) and TGN (golgin-97) markers. VSVG-YFP colocalized with both perinuclear and satellite Golgi structures (Fig. S1, available at http://www.jcb.org/cgi/content/full/jcb.200712137/DC1); however, neither Golgi nor TGN markers were observed within the cleavage furrow where EMMA punctae were seen, suggesting

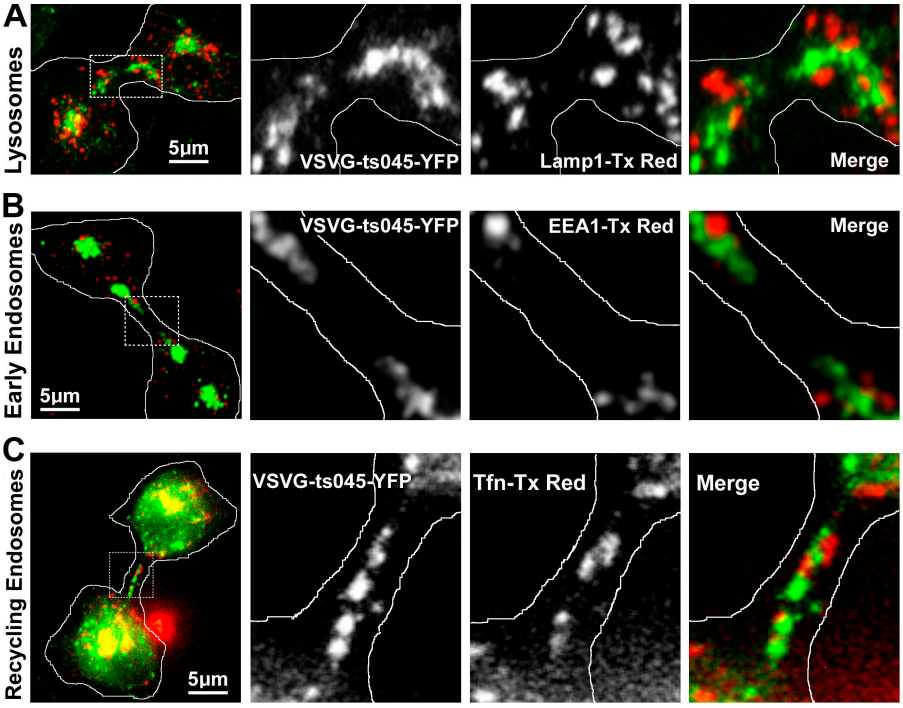

Figure 2. **Accumulation of VSVG-YFP–labeled post-Golgi exocytic membrane is distinct from other membrane compartments.** (A and B) Hela cells expressing VSVG-YFP (green) were fixed 60 min after transfer to 32°C and immunostained with α–Lamp-1 for lysosomes (A, red) or α-EEA1 for early endosomes (B, red). (C) BSC1 cells expressing both transferrin receptor and VSVG-YFP (green) were pulse labeled with 5 mg/ml Texas red–conjugated transferrin (red) after transfer to 32°C and chased for 15 min with transferrin-free media before imaging by SDCM. Dashed rectangles indicate enlarged regions shown in adjacent panels.

that post-Golgi cargo are responsible for the accumulations. Even though EMMA punctae are large (~2–5 μm in diameter) and pleomorphic, light microscopy of fixed specimens cannot resolve whether they are single structures or an accumulation of vesicles.

We next examined the distribution of post-Golgi exocytic membrane accumulations (EMMA punctae) relative to the midbody, as it was previously proposed that only one daughter cell contributes membrane to the cleavage furrow (Gromley et al., 2005). Curiously, we found that even in pulse-chase–labeled cells, the cargo distribution was highly variable and fell into three groups. A third of cells had no accumulations, a third had accumulations only on one side (asymmetrical), and a third was symmetrically positioned on both sides of the furrow (Fig. 1). One rationalization of this heterogeneous distribution is that as cytokinesis occurs over several hours (Gromley et al., 2005; Chen et al., 2006) and fixed assays only provide a random snapshot, membrane accumulations could potentially transition between these three states during cytokinesis.

Accumulations of post-Golgi membrane within the cleavage furrow are distinct from other membrane compartments

Assorted membranous organelles, ranging from recycling endosomes to lysosomes, have been suggested to play an active role in cytokinesis (Finger and White, 2002; Schweitzer et al., 2005; Gromley et al., 2005; Chen et al., 2006). To explore how these organelles are positioned relative to the furrow and post-Golgi cargo, we labeled these structures in fixed cells. Consistent with other reports, we found that a population of Lamp1-labeled lysosomes, EEA1-labeled early endosomes, and transferrin-labeled recycling endosomes localize to the cleavage furrow during cytokinesis (Fig. 2). However, colocalization analysis revealed that a majority of post-Golgi membrane accumulations within the furrow remain distinct from these intracellular compartments (Fig. 2): only 3.5% of VSVG-YFP colocalizes with lysosomes, 9.7% with early endosomes, and 7.9% with recycling endosomes. Thus, although many organelles, including lysosomes, endosomes, and satellite Golgi, are in or adjacent to the furrow, these organelles remain distinct from EMMA of post-Golgi vesicles. We note that recycling endosomes appear to be more proximal to the midbody than other endocytic organelles, which is consistent with previous findings (Finger and White, 2002; Glotzer, 2005; Schweitzer et al., 2005).

Post-Golgi membrane vesicles are directed to the cleavage furrow from both daughter cells during cytokinesis

To examine post-Golgi membrane trafficking in live cells, we rapidly acquired 3D confocal stacks (10 optical sections) every 5 s using SDCM. This approach enabled us to visualize the paths of individual VSVG-YFP–labeled vesicles as they left the Golgi and traveled to the plasma membrane. As seen in the representative time-lapse sequence in Fig. 3 C, vesicles from both daughter cells trafficked into the furrow region (Videos 1 and 2, available at http://www.jcb.org/cgi/content/full/jcb.200712137/DC1). To demonstrate bilateral trafficking into the furrow, we traced the paths of 20 post-Golgi vesicles from each daughter cell that targeted the furrow (Fig. 3 B and Videos1 and 2). In total, 43 post-Golgi vesicles were seen to traffic into the cleavage furrow from the upper daughter cell and 52 were observed in the lower daughter cell. In both daughter cells, vesicles traveled along curvilinear paths and in rapid (up to 1 μm/s) stop-and-go motion reminiscent of trafficking along microtubules. Similar results were seen using YFP-labeled glycosylphosphatidylinositol

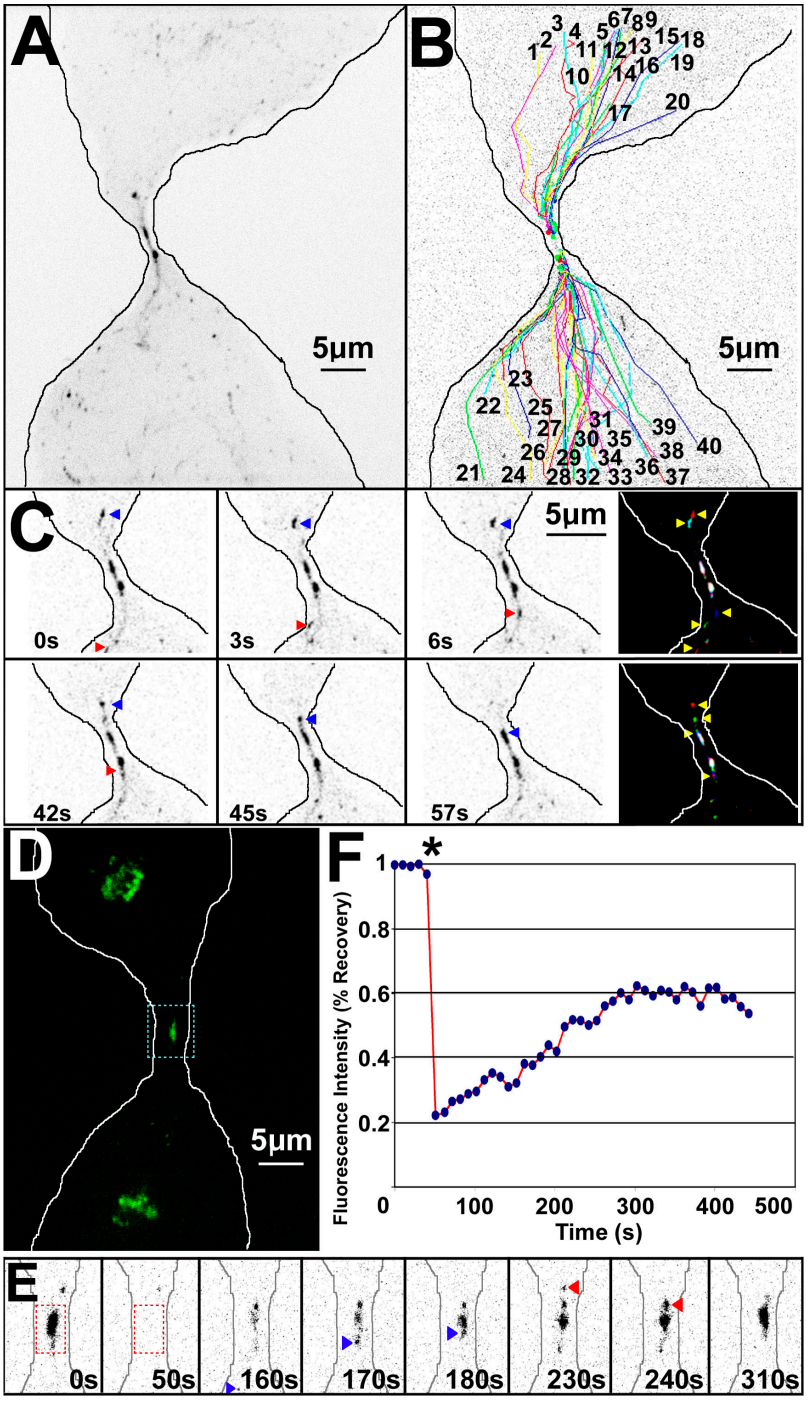

Figure 3. **SDCM and FRAP analysis reveals that post-Golgi vesicles are directed to the cleavage furrow from both daughter cells and form accumulations of individual vesicles.** (A) BSC1 cells expressing VSVG-YFP were imaged live by SDCM, with one confocal stack acquired every 5 s (Video 1, available at http://www.jcb.org/cgi/content/full/jcb.200712137/DC1). (B) Paths of 20 post-Golgi vesicles from each daughter cell were manually tracked (Video 2, available at http://www.jcb.org/cgi/content/full/jcb.200712137/DC1). (C) Individual paths of two vesicles (one from each daughter cell) are indicated with blue and red arrowheads and shown in RGB merge. Yellow arrowheads show highlighted vesicles in adjacent frames. (D) BSC1 cells expressing VSVG-YFP (green) were imaged by SDCM (one confocal stack every 10 s). Dashed rectangles indicate enlarged region shown in E. (E) Time-lapse fluorescence imaging reveals fluorescence recovery in photobleached ROI (dashed rectangles). Individual vesicles trafficking into bleached area from both daughter cells are denoted by blue and red arrowheads (Video 4, available at http://www.jcb.org/cgi/content/full/jcb.200712137/DC1). (F) Quantification of FRAP kinetics (asterisk demarks bleaching period of ~3 s).

(GPI)-anchored protein, supporting that this represents a general constitutive membrane trafficking pathway (Fig. S2 and Video 3, available at http://www.jcb.org/cgi/content/full/jcb.200712137/DC1).

Together, these findings suggest that both daughter cells contribute post-Golgi vesicles to the furrow during cytokinesis. Additionally, although we initially observe symmetric accumulation of post-Golgi vesicles in the furrow, after 18 min there is a transition to an asymmetrical accumulation (Video 1). This transition suggests that membrane accumulations (symmetric vs. asymmetrical) can vary during cytokinesis and is consistent with the different states observed in Fig. 1.

Although symmetric membrane trafficking to the cleavage furrow during mammalian cytokinesis differs from the previous asymmetrical model, there is precedent for symmetric membrane trafficking during cytokinesis in plants (Jurgens, 2005). In plant cells, post-Golgi vesicles from both daughter cells are directed toward the cell plate region between daughter cells and through homotypic fusion form the phragmoplast, which expands and ultimately fuses with the outer membrane to separate the two cells (Staehelin and Hepler, 1996; Otegui et al., 2005). Our studies suggest that similar to plant cells, mammalian cells can symmetrically polarize membrane traffic to the cleavage furrow during cytokinesis.

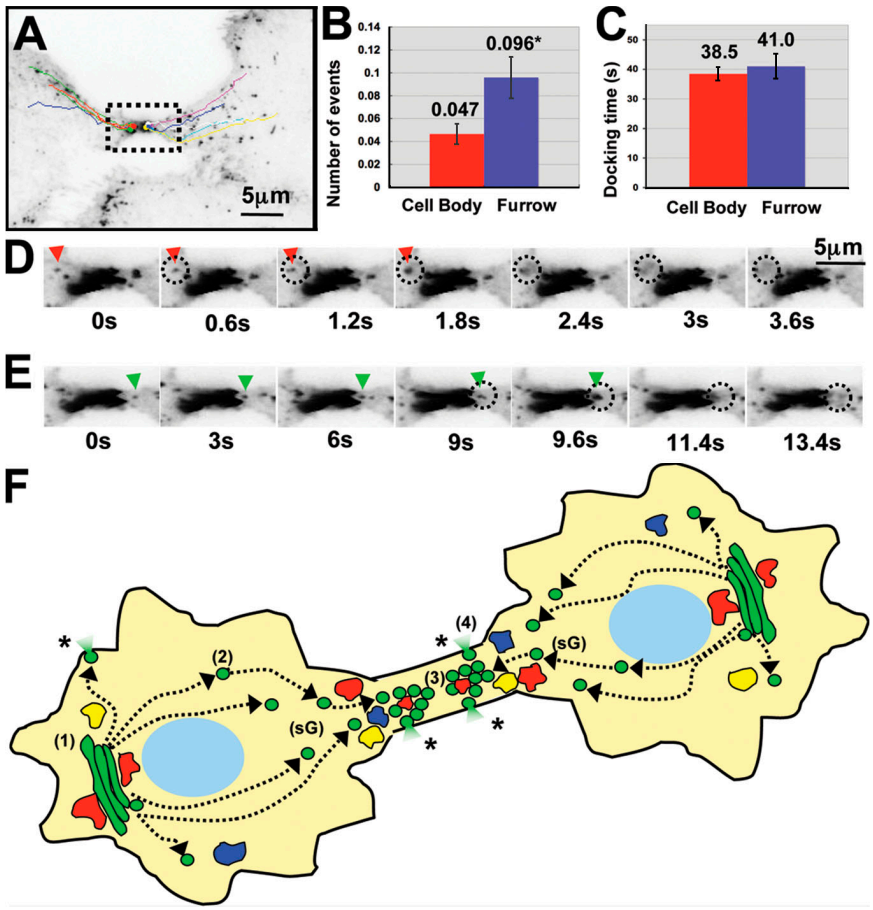

Figure 4. **TIRFM analysis reveals exocytosis of post-Golgi vesicles from both daughter cells at the cleavage furrow during cytokinesis.** (A) BSC1 cells expressing VSVG-YFP were imaged by TIRFM at 1.67 frames/s (Video 5, available at http://www.jcb.org/cgi/content/full/jcb.200712137/DC1). Paths of five vesicles are shown from each daughter cell as they enter the furrow region. Dashed rectangle indicates enlarged regions shown in D and E. (B) The number of exocytic events in the furrow and cell body was manually determined and displayed as number of events per μm^2 per minute. Error bars show SEM. (C) Docking times (in seconds) of individual vesicles before fusion with plasma membrane were determined in cell body and cleavage furrow regions. Error bars show SEM. (D and E) Gallery of enlarged TIRFM images from A shows exocytic fusion of vesicles on both sides of midbody region (red and green arrowheads). Dashed circles indicate sites of exocytic fusion. (F) Working model for membrane trafficking during cytokinesis. Individual post-Golgi (1) vesicles (green) from both daughter cells traffic to furrow region (2) where they accumulate (3) and remain distinct from lysosomes (yellow), early endosomes (dark blue), and recycling endosomes (red). Post-Golgi vesicles from both daughter cells can exocytose (4) at the furrow (asterisks). Golgi, green; nucleus, light blue.

FRAP analysis suggests that post-Golgi membrane accumulations within the cleavage furrow consist of individual vesicles

To determine whether the post-Golgi membrane accumulations observed at the furrow consist of a collection of individual vesicles or a large compartment comprised of homotypically fused post-Golgi vesicles (as in the plant phragmoplast), we photobleached EMMA punctae and monitored FRAP by SDCM (Fig. 3, D–F; and Video 4, available at http://www.jcb.org/cgi/content/full/jcb.200712137/DC1). If vesicles fuse with a preexisting, photobleached structure upon arrival at the furrow, the fluorescent signal should dissipate upon fusion as VSVG cargo diffuses throughout the compartment. Alternatively, if vesicles do not fuse with a compartment, no dissipation will be seen and individual vesicles should be observed. After photobleaching EMMA in the furrow of BSC1 cells, post-Golgi vesicles were seen to traffic into the furrow from both daughter cells. Notably, after reaching the midbody region they persisted as individual vesicles (Fig. 3 E, 170 s). The kinetics of FRAP (Fig. 3 F) were slow ($t_{1/2}$ ~100 s), which supports a model whereby individual vesicles accumulate in the midbody region, as previously proposed (Gromley et al., 2005).

Exocytosis from both daughter cells occurs at the cleavage furrow during cytokinesis

Arguably, vesicles that accumulate in the furrow region may not fuse, and their disappearance may simply reflect trafficking to other regions of the cell. To determine whether post-Golgi vesicles that traffic into the furrow can fuse directly with the plasma membrane, we used TIRFM imaging. Visualizing exocytosis at the cleavage furrow by TIRFM might seem unlikely, as this region is generally suspended between daughter cells (Gromley et al., 2005). However, the flat and elongated morphology of the furrow of BSC1 cells enabled us to occasionally visualize it by TIRFM.

BSC1 cells expressing VSVG-YFP were imaged, and the tracks of 10 post-Golgi vesicles are shown entering the cleavage furrow (Fig. 4 A). Video 5 (available at http://www.jcb.org/cgi/content/full/jcb.200712137/DC1) clearly demonstrates post-Golgi vesicle trafficking into the furrow from both daughter cells, which is consistent with our SDCM observations (Fig. 3 B and Videos 1 and 2). Furthermore, we again detect a transition from symmetric EMMA at the onset of imaging to asymmetrical EMMA (Video 5, 860 s).

Importantly, we observed a characteristic exocytic "flash" when vesicles fused with the plasma membrane (Fig. 4, D and E; Fig. S3; and Videos 5, 6, and 7, available at http://www.jcb.org/cgi/content/full/jcb.200712137/DC1). Fusion events were observed on both sides of the cleavage furrow, which indicates that not only are vesicles capable of trafficking into the midbody region from both daughter cells but that they can exocytose upon arrival. We mapped exocytic fusion sites to determine whether there was indeed an increase in vesicle fusion events within the furrow. Quantitative analysis of the spatial distribution of

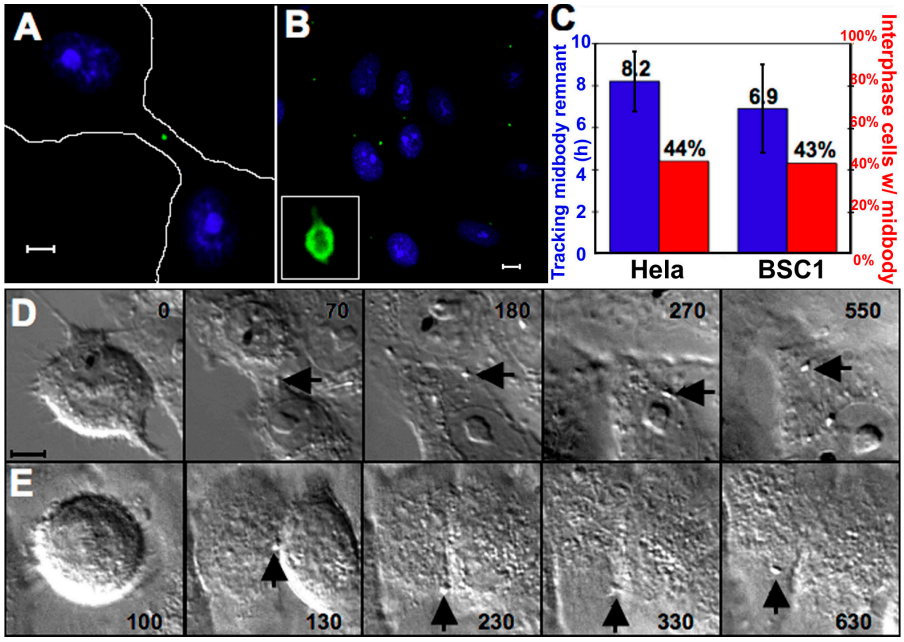

Figure 5. **The cytokinesis midbody is asymmetrically inherited by one daughter cell.** (A and B) Hela or BSC1 cells were fixed and immunostained with α-MKLP1. (A and B) During cytokinesis (A), MKLP1 localizes to the midbody structure (periphery of the dividing cell outlined in white), and after completion of cytokinesis, MKLP1 is found in ring-like structures in interphase cells (B), which is shown in the high magnification inset (box width, 2 μm). (C) Quantification of percentage of interphase Hela and BSC1 cells with a midbody remnant by MKLP1 immunostaining (right y-axis, red; $n = 355$ Hela cells and $n = 375$ BSC1 cells). Error bars show SD. (D) Time-course gallery of midbody inheritance in BSC1 cells at completion of cytokinesis (Video 8, available at http://www.jcb.org/cgi/content/full/jcb.200712137/DC1). The midbody is indicated by arrows (time in minutes). (E) Time-course of midbody inheritance in Hela cells at completion of cytokinesis (Video 9, available at http://www.jcb.org/cgi/content/full/jcb.200712137/DC1). The midbody is indicated by arrows (time in minutes). Bars, 5 μm.

exocytic sites (Fig. 4 B) revealed twice as many fusion events in the cleavage furrow (0.096 events/μm^2/min) relative to the cell body (0.047 events/μm^2/min).

As many membrane trafficking components linked to vesicle docking and fusion have been shown to localize to the furrow (Low et al., 2003; Gromley et al., 2005; Konopka et al., 2006), we analyzed whether vesicle docking kinetics are different in the furrow relative to the cell body. Vesicle docking was operationally defined as the period of time a vesicle is immobile (remained within 1-μm radius) at the plasma membrane before exocytic fusion. The mean docking times were ~40 s and were similar in the two regions (Fig. 4 C), indicating that a difference in morphological tethering/docking, for example, by the exocyst complex, is unlikely to be responsible for enhanced vesicle fusion near the furrow (Fig. 4 B).

There are two explanations that may account for the differences of our results with the previously described asymmetrical membrane trafficking model (Gromley et al., 2005). First, the former study acquired confocal stacks every 5 min, which allowed for visualization of cytokinesis in its entirety, but prevented direct monitoring of real-time dynamics of vesicle trafficking and exocytosis. In this study, confocal stacks were acquired 60-fold faster (albeit for a smaller time window), which allowed direct visualization and tracking of the origin, dynamics, and fate of post-Golgi vesicles during cytokinesis. This higher temporal-spatial view indicates that multiple small vesicles traffic into EMMA punctae, which may serve as a secondary releasable pool. A second interpretation, which is parsimonious with the view that cytokinesis is asymmetrical (Gromley et al., 2005), is that the long process of cytokinesis may be subdivided into three functional stages: furrow ingression (no membrane trafficking), and then symmetric membrane trafficking, followed by asymmetrical membrane trafficking. This new working model is consistent with our data that there either was no accumulation, symmetric EMMA punctae, or asymmetrical EMMA (Fig. 1). Our live cell SDCM and TIRFM support this concept, as we observed a transition from symmetric post-Golgi EMMAs to asymmetrical EMMAs (Videos 1 and 5) during cytokinesis.

The ultimate fate of the midbody is not clear, as some studies have implicated asymmetrical inheritance (Mishima et al., 2002; Gromley et al., 2005), whereas other studies suggest that the midbody is discarded (Golsteyn et al., 1994; Hinchcliffe, 2005; Dubreuil et al., 2007), prompting us to examine this issue in both BSC1 and Hela cells using live cell imaging and quantitative analysis. Using immunofluorescence of the midbody marker protein MKLP1 (Fig. 5, A and B; Mishima et al., 2002), we observed that the midbody structure persists after the completion of cytokinesis in 43% of BSC1 (160 MKLP1 punctae/375 nuclei) and 44% of Hela (157 MKLP1 punctae/355 nuclei) interphase cells (Fig. 5, B and C). We observed multiple MKLP1 punctae in <5% of interphase cells. To further examine midbody inheritance, we used DIC microscopy for long-term imaging of Hela and BSC1 cells to track the fate of the midbody (visible by both DIC and phase-contrast microscopy). For both cell lines, we observed asymmetrical midbody inheritance into one daughter cell after cytokinesis (Fig. 5, D and E; and Videos 8 and 9, available at http://www.jcb.org/cgi/content/full/jcb.200712137/DC1) and persistence of this structure for many hours (Fig. 5 C). This finding of asymmetrical midbody inheritance supports a parsimonious interpretation of our data with previous asymmetrical models (Gromley et al., 2005).

Mechanisms that lead to stabilization of the novel EMMA structures, which we herein characterize, are unknown, although a new multifunctional protein called BRUCE may act as a regulator of membrane delivery (Pohl and Jentsch, 2008). Both the trafficking and accumulations suggest parallels with plant phragmoplasts, which are also believed to be of post-Golgi origin (Staehelin and Hepler, 1996; Otegui et al., 2005). However, our FRAP studies suggest a principle difference between mammalian EMMA structures and the plant phragmoplast in that in the

former, accumulated vesicles do not fuse with each other, an observation which will ultimately require high resolution ultrastructure (e.g., electron tomography) to verify.

In conclusion, this paper provides new insight into post-Golgi vesicle dynamics during cytokinesis (Fig. 4 F). Using fast SDCM imaging, we show that both daughter cells can contribute membrane to the cleavage furrow during cytokinesis. These individual vesicles accumulate in the midbody region, where they maintain their identity and remain distinct from other membranous organelles. Finally, using TIRFM, we observed trafficking of post-Golgi vesicles from both daughter cells and preferential exocytosis near the furrow.

Materials and methods

Cell culture and VSVG-YFP fluorescence labeling

BSC1 and Hela cells were grown in DME (American Type Culture Collection) supplemented with 10% FBS, 1% penicillin/streptomycin, 1% L-glutamine, and 1% nonessential amino acids (Invitrogen). Cells were cultured at 37°C (unless otherwise noted), supplemented with 5% CO_2, and plated on dishes (Mattek) before imaging. For VSVG-YFP and YFP-GPI expression, BSC1 and Hela cells were infected with adenovirus as previously described (Toomre et al., 2000). YFP-GPI–infected cells were incubated at 19°C for 2 h before imaging.

Immunofluorescence and VSVG/transferrin labeling

BSC1 and Hela cells expressing VSVG-YFP (ts045 with spacer; Toomre et al., 2000) were released from the 39°C temperature-sensitive block for 60 min, permeabilized with 0.1% Triton X-100 and 4% PFA for 30 s, and fixed in 4% PFA with 0.02% glutaraldehyde for 20 min at room temperature. Cells were washed with PBS and immunostained with mouse anti-tubulin (Sigma-Aldrich), mouse α-EEA1 (BD Biosciences), or mouse α-LAMP1 (BD Biosciences) antibodies, followed by donkey α-mouse Cy5 or donkey α-mouse Texas red (Jackson ImmunoResearch Laboratories) secondary antibodies, and imaged with SDCM. For midbody immunofluorescence, cells were fixed on ice with ethanol for 15 min, and immunostained with rabbit α-MKLP1 (Santa Cruz Biotechnology, Inc.) and HOECHST 15090 dye (Serva) followed by donkey α-rabbit Cy2 (Jackson ImmunoResearch Laboratories). All confocal images shown are 2D projections of confocal stacks (typically ∼10 sections; 0.5-µm intervals). For VSVG/transferrin colabeling, BSC1 cells were coinfected with adenoviruses separately expressing VSVG-YFP and transferrin receptor for 1 h at 37°C. Cells were washed with PBS and incubated in DME for 9–12 h at 39.5°C before imaging. Cells were transferred to 32°C for 15 min before adding a pulse of 5 mg/ml transferrin–Texas red (Invitrogen) for 5 min. Cells were washed with PBS and incubated in DME at 32°C for an additional 15 min before live imaging of both fluorophores with SDCM.

Microscopy

For ultra-sensitive 4D imaging (3D + time) a Yokagawa-type SDCM system equipped with a FRAP photokinesis unit was used (PerkinElmer). The system was mounted onto an inverted microscope (IX71; Olympus) equipped with a 1 Kb × 1 Kb electron-multiplying charge-coupled device camera (Hamamatsu Photonics) and a temperature-controlled stage set at 32°C, which was controlled by Ultraview ERS software (PerkinElmer). Samples were imaged in phenol red–free DME by a 60× 1.4 NA oil phase objective, yielding a spatial resolution of 0.14 µm per pixel. Excitation was achieved using 514-nm argon and 568-nm argon/krypton lasers (Melles Griot). Exposure times were 0.1–0.25 s. TIRFM images were acquired using an inverted microscope equipped with a 1.45 NA 60× TIRFM lens (Olympus), back-illuminated electron-multiplying charge-coupled device camera (512 × 512, 16-bit; iXon887; Andor Technologies), and controlled by Andor iQ software (Andor Technology). Excitation was achieved using a 514-nm line of argon laser, and exposure times were 0.1–0.2 s and acquired at 0.5–4 Hz. The calculated evanescent field depth was ∼100 nm. DIC images were acquired using either a 60× 1.2 NA water immersion objective or 60× 1.42 NA oil immersion objective, with an aluminum closed cell chamber that uses two 15-mm coverslips, and a BX-51 microscope (Olympus) with Nomarski optics, all enclosed within an Air-therm temperature-regulated environmental box at 37°C. Exposure times were 1 s, and two to four images were acquired per minute with an iXon887 electron-multiplying charge-coupled device camera.

FRAP experiments

A photokinesis unit mounted on the SDCM (described in Microscopy) was used for FRAP experimentation and controlled by Ultraview ERS software. Regions of interest (ROI) were identified and photobleached with a 514-nm argon laser at 100% power for 200 bleach cycles (∼3–5 s). Quantification of fluorescence recovery was obtained using Ultraview ERS software programs.

Image analysis

Ultraview ERS software was used to subtract background of images before analysis by Image J software (National Institutes of Health). No nonlinear algorithms were used to alter fluorescent signals. Colocalizations were quantified for numerous ROI that corresponded to EMMA on a pixel-per-pixel basis using Imaris (Biplane AG) automated software.

Online supplemental material

Fig. S1 shows that post-Golgi vesicles in the cleavage furrow are distinct from satellite Golgi. Fig. S2 shows that SDCM analysis of YFP-GPI–labeled post-Golgi vesicles indicates trafficking into the cleavage furrow from both daughter cells. Fig. S3 shows that quantitative imaging of VSVG-YFP in BSC1 cells by TIRFM differentiates between vesicles that leave the evanescent field and those that dock and fuse. Video 1 shows that SDCM analysis reveals that post-Golgi vesicles are directed to the cleavage furrow from both daughter cells (QuickTime video from Fig. 3 A). Video 2 shows manual tracking of post-Golgi vesicles that are directed to the cleavage furrow from both daughter cells (QuickTime video from Fig. 3 B). Video 3 shows that SDCM analysis reveals that YFP-GPI–labeled post-Golgi vesicles are directed to the cleavage furrow from both daughter cells. Video 4 shows that FRAP analysis suggests that post-Golgi membrane accumulations in the cleavage furrow consists of individual vesicles (QuickTime video from Fig. 3 E). Video 5 shows that TIRFM analysis reveals exocytosis of post-Golgi vesicles from both daughter cells at the cleavage furrow (QuickTime video from Fig. 4, A, D, and E). Video 6 shows that TIRFM analysis reveals exocytosis of post-Golgi vesicles from both daughter cells at the cleavage furrow. Video 7 shows that TIRFM analysis reveals exocytosis of post-Golgi vesicle at the cleavage furrow. Video 8 shows that DIC time-lapse imaging indicates asymmetrical midbody inheritance in BSC1 cells (QuickTime video from Fig. 5 D). Video 9 shows that DIC time-lapse imaging indicates asymmetrical midbody inheritance in Hela cells (QuickTime video from Fig. 5 E). Online supplemental material is available at http://www.jcb.org/cgi/content/full/jcb.200712137/DC1.

We thank J. Bogan, F. Gorelick, and R. Perera for their comments.

This research was supported by a Human Frontier Science Program grant (RGY40/2003) and National Institutes of Health award (1DP2OD002980-01) to D. Toomre and Predoctoral Training Grant (T32 GM07223) and Anna Fuller Fellowship to J. Goss. We thank Olympus for supporting TIRFM equipment.

Submitted: 21 December 2007
Accepted: 28 May 2008

References

Chen, X.W., M. Inoue, S.C. Hsu, and A.R. Saltiel. 2006. RalA-exocyst-dependent recycling endosome trafficking is required for the completion of cytokinesis. *J. Biol. Chem.* 281:38609–38616.

Danilchik, M.V., S.D. Bedrick, E.E. Brown, and K. Ray. 2003. Furrow microtubules and localized exocytosis in cleaving *Xenopus laevis* embryos. *J. Cell Sci.* 116:273–283.

Dubreuil, V., A. Marzesco, D. Corbeil, W.B. Huttner, and M. Wilsch-Brauninger. 2007. Midbody and primary cilium of neural progenitors release extracellular membrane particles enriched in the stem cell marker prominin-1. *J. Cell Biol.* 176:483–495.

Eggert, U.S., T.J. Mitchison, and C.M. Field. 2006. Animal cytokinesis: from parts list to mechanisms. *Annu. Rev. Biochem.* 75:543–566.

Finger, F.P., and J.G. White. 2002. Fusion and fission: membrane trafficking in animal cytokinesis. *Cell.* 108:727–730.

Gaietta, G.M., B. Giepmans, T.J. Deerinck, W.B. Smith, L. Ngan, J. Llopis, S.R. Adams, R.Y. Tsien, and M.H. Ellisman. 2006. Golgi twins in late mitosis revealed by genetically encoded tags for live cell imaging and correlated electron microscopy. *Proc. Natl. Acad. Sci. USA.* 103:17777–17782.

Glotzer, M. 2005. The molecular requirements for cytokinesis. *Science.* 307:1735–1739.

Golsteyn, R.M., S.J. Schultz, J. Bartek, A. Ziemiecki, T. Ried, and E.A. Nigg. 1994. Cell cycle analysis and chromosomal localization of human Plk1, a putative homologue of the mitotic kinases *Drosophila* polo and *Saccharomyces cerevisiae* Cdc5. *J. Cell Sci.* 107:1509–1517.

Gromley, A., C. Yeaman, J. Rosa, S. Redick, C.T. Chen, S. Mirabelle, M. Guha, J. Sillibourne, and S.J. Doxsey. 2005. Centriolin anchoring of exocyst and SNARE complexes at the midbody is required for secretory-vesicle-mediated abscission. *Cell.* 123:75–87.

Hill, E., M. Clarke, and F.A. Barr. 2000. The Rab6-binding kinesin, Rab6-KIFL, is required for cytokinesis. *EMBO J.* 19:5711–5719.

Hinchcliffe, E.H. 2005. Using long-term time-lapse imaging of mammalian cell cycle progression for laboratory instruction and analysis. *Cell Biol. Educ.* 4:284–290.

Jurgens, G. 2005. Cytokinesis in higher plants. *Annu. Rev. Plant Biol.* 56:281–299.

Konopka, C.A., J.B. Schleede, A.R. Skop, and S.Y. Bednarek. 2006. Dynamin and cytokinesis. *Traffic.* 7:239–247.

Lecuit, T., and E. Wieschaus. 2000. Polarized insertion of new membrane from a cytoplasmic reservoir during cleavage of the *Drosophila* embryo. *J. Cell Biol.* 150:849–860.

Low, S.H., X. Li, M. Miura, N. Kudo, B. Quinones, and T. Weimbs. 2003. Syntaxin 2 and endobrevin are required for the terminal step of cytokinesis in mammalian cells. *Dev. Cell.* 4:753–759.

Mishima, M., S. Kaitna, and M. Glotzer. 2002. Central spindle assembly and cytokinesis require a kinesin-like protein/RhoGAP complex with microtubule bundling activity. *Dev. Cell.* 2:41–54.

Niswonger, M.L., and T.J. O'Halloran. 1997. A novel role for clathrin in cytokinesis. *Proc. Natl. Acad. Sci. USA.* 94:8575–8578.

Otegui, M.S., K.J. Verbrugghe, and A.R. Skop. 2005. Midbodies and phragmoplasts: analogous structures involved in cytokinesis. *Trends Cell Biol.* 15:404–413.

Pohl, C., and S. Jentsch. 2008. Final stages of cytokinesis and midbody ring formation are controlled by BRUCE. *Cell.* 132:832–845.

Schweitzer, J.K., E.E. Burke, H.V. Goodson, and C. D'Souza-Schorey. 2005. Endocytosis resumes during late mitosis and is required for cytokinesis. *J. Biol. Chem.* 280:41628–41635.

Shima, D.T., N. Cabrera-Poch, R. Pepperkok, and G. Warren. 1998. An ordered inheritance strategy for the Golgi apparatus: visualization of mitotic disassembly reveals a role for the mitotic spindle. *J. Cell Biol.* 141:955–966.

Skop, A.R., D. Bergmann, W.A. Mohler, and J.G. White. 2001. Completion of cytokinesis requires a brefeldin A-sensitive membrane accumulation at the cleavage furrow apex. *Curr. Biol.* 11:735–746.

Skop, A.R., H. Lin, J. Yates, B.J. Mayer, and R. Heald. 2004. Dissection of the mammalian midbody proteome reveals conserved cytokinesis mechanisms. *Science.* 305:61–66.

Staehelin, L.A., and P.K. Hepler. 1996. Cytokinesis in higher plants. *Cell.* 84:821–824.

Toomre, D., J.A. Steyer, P. Keller, W. Almers, and K. Simons. 2000. Fusion of constitutive membrane traffic with the cell surface observed by evanescent wave microscopy. *J. Cell Biol.* 149:33–40.

Warner, A.K., J.H. Keen, and Y.L. Wang. 2006. Dynamics of membrane clathrin-coated structures during cytokinesis. *Traffic.* 7:205–215.

Wilson, G.M., A.B. Fielding, G.C. Simon, X. Yu, P.D. Andrews, R.S. Hames, A.M. Frey, A.A. Peden, G.W. Gould, and R. Prekeris. 2005. The FIP3-Rab11 protein complex regulates recycling endosome targeting to the cleavage furrow during late cytokinesis. *Mol. Biol. Cell.* 16:849–860.